Supplemental Methods

Generation of GL261 cells expressing the SIINFEKL peptide

The SIINFEKL sequence was amplified using the following primers: 5′-GCAATTGAACCGGTGCC-3′ and 5′-TTTGAGGAATTCTTACAGTTTTTCAAAGTTGATTATACTCATGGTGGCAAGCTTAAG GATCCTCACGACACCTG-3′ utilizing the lentivirus backbone pLV-EF1a-IRES-Puro vector (Addgene, Cambridge, MA, USA). The amplified SIINFEKL-encoding fragments and third-generation lentiviral plasmid pLV-EF1a-IRES-Puro vector (Addgene) were digested using the AgeI and EcoRI restriction enzymes (Enzynomics, Daejeon, Korea). The two digested DNA fragments were ligated using T4 DNA ligase (NEB, Ipswich, MA, USA), and the plasmid was amplified using Stbl3 competent cells (Invitrogen, Waltham, MA, USA). For lentivirus production, Lenti-X™ 293 T cells (Takara Bio, Shiga, Japan) were transfected with third-generation lentiviral packaging plasmids (pMDLg/pRRE, pRSV-Rev and pMD2.G; Addgene) and a SIINFEKL-encoding plasmid using Lipofectamine 3000 (Thermo Fisher Scientific, Hampton, NH, USA) according to the manufacturer's instructions. After 42 hours of incubation at 37°C with 95% humidity and 5% CO_2 in a cell culture incubator, the supernatant containing lentivirus was harvested and filtered through 45-μm filters (Sartorius, Göttingen, Germany). The SIINFEKL-encoding lentiviral supernatant was applied to GL261 tumor cells along with protamine sulfate (Sigma–Aldrich, St. Louis, MO, USA) and spinoculated by centrifugation at 32°C and 1000 g for 1 hour. After 1 day, transduced GL261 cells were subcultured in fresh complete media. Following confirmation of SIINFEKL-MHC class I expression, transduced cells were selected by puromycin treatment. SIINFEKL-MHC class I expression on transduced cells was confirmed using an APC anti-mouse H-2Kb-bound SIINFEKL antibody (BioLegend,

San Diego, CA, USA) through flow cytometry.

Syngeneic mouse GBM model

During the inoculation procedure, mice were anesthetized using isoflurane inhalation. The mice were placed on a heating pad to maintain their body temperature throughout the procedure. The head was immobilized using a stereotactic device (Stoelting Co, Wood Dale, IL, USA) and sterilized with 70% alcohol. Subsequently, a midline incision was performed on the skin overlaying the cranial vault. The skin was incised to reveal the skull, and a 2-mm hole was created 2 mm to the right and 2 mm anterior to the bregma utilizing a stereotactic device. Diluted cells were dispensed into a Hamilton syringe (The Hamilton Company, Reno, NV, USA) and administered at a flow rate of 0.4 µL/minute over 5 minutes utilizing a nano-injector (KD Scientific, Holliston, MA, USA) at a depth of 3 mm below the brain surface. A total of 1×10^5 cells were inoculated. Following the injection, the aperture in the skull was closed using an adhesive, and the skin was sutured with a 7-mm wound clip (Ro-boz, Gaithersburg, MD, USA). The incision site was sterilized once more, and oxygen supplementation was administered as the mouse recuperated on a heating pad.

Single-cell preparation of immune and tumor cells

For the single-cell preparation, the tumor tissues were initially fragmented into small sections before undergoing an automated dissociation process. The gentleMACS Octo Dissociator (Miltenyi Biotec, Auburn, CA, USA) was used with the program 37°C_mTDK_1, followed by filtering the resulting mixture through 70-µm cell strainers (SPL, Pocheon, Korea). The cells collected post-filtration were resuspended in 5 mL of 30% Percoll mixed with DMEM complete medium. Subsequently, the cells were layered onto 3 mL of 70% Percoll containing DPBS supplemented with 1% bovine serum. Immune cells were then isolated via centrifugation without the application of a brake. Following the removal of the Percoll layer, the cells

underwent washing with 5 mL of DPBS with 1% bovine serum albumin and were subsequently treated with ammonium-chloride-potassium lysis buffer to eradicate red blood cells. The collected immune cells were subsequently filtered through a 70-µm cell strainer.

For the examination of TdLNs and spleens, single-cell suspensions were generated by mechanically disaggregating lymph nodes using a 70-µm nylon mesh cell strainer (SPL) and subsequently treated with ACK lysis buffer. In the tumor cell density assessment using GL261-GFP cells, tumor cells were extracted from a single-cell suspension. The filtered cells were resuspended in a 30% Percoll solution and centrifuged to eliminate the supernatant, and the resultant pellet, which contained tumor cells, was preserved for subsequent utilization.

Flow cytometry

To evaluate the binding of *in vivo*-administered anti-PD-1 antibody, single-cell suspensions of processed tissues were washed with FACS buffer and incubated with a goat anti-rat IgG antibody labeled with Cy5-fluorochrome (Jackson ImmunoResearch, West Grove, PA, USA) for 30 minutes at 4°C. Subsequently, the cells were washed, and surface staining was carried out. For the fluorescence minus one control, anti-rat IgG with labels was added.

For transcription factor staining, surface staining was conducted, followed by fixation and permeabilization using Fix/Perm buffer (BioLegend) and Perm buffer (BioLegend) as per the manufacturer's instructions. The cells were then stained with antibodies against intracellular proteins, including TCF1 (AF488, Cell signaling Technology, Danvers, MA, USA, C63D9), TOX (PE, Thermo Fisher Scientific, TXRX10; APC, Miltenyi Biotech, REA473), and anti-Ki67 (FITC, BioLegend, 16A8; PE, Thermo Fisher Scientific, SolA15), for 30 minutes at 4°C.

For cytokine staining, cells were pre-incubated at 37°C with 5% CO_2 in Roswell Park Memorial Institute medium (RPMI, Corning), 10% FBS, 50 ng/mL phorbol-myristate acetate (PMA,

Sigma), 1 µg/mL ionomycin (Sigma), 1 mM GolgiStop (BD Biosciences, San Jose, CA, USA), and 1 mM GolgiPlug (BD Biosciences) for 4 hours at 37°C in the dark. Surface staining was conducted, and then a Fixation/Permeabilization Solution Kit (BD Biosciences, 554714) was utilized. The cells were then stained with antibodies against intracellular proteins, including IFN-γ (APC, BioLegend, XMG1.2), TNF-α (APC-Cy7, BioLegend MP6-XT22), and CD107a (PE-Cy7, BD Biosciences, ID4B), for 30 minutes at 4°C. All samples were analyzed using an LSRFortessa system (BD Biosciences), and the data were processed with FlowJo software (Tree Star, San Carlos, CA, USA).

Depletion of CD8 T cells *in vivo*

To deplete CD8 T cells *in vivo*, an anti-mouse CD8 depletion antibody (BioXCell, 2.43) or an isotype-matched control (BioXCell, LTF-2) was diluted in 200 µL of DPBS and intraperitoneally injected on days −2, −1, 7, 14, and 21 relative to tumor cell implantation.

Single-cell RNA sequencing

A count matrix was produced using Cell Ranger (10x Genomics, Pleasanton, CA, USA). R version 4.2 (https://www.r-project.org/) and the R package Seurat v4.1.1 (https://satijalab.org/seurat/) were employed for single-cell RNA sequencing data analysis. Cells of poor quality were eliminated based on the following specific criteria: nFeature_RNA < 300, nFeature_RNA > 4,000, nCount_RNA > 20,000, or percent.mt > 20. The filtered data were normalized using the NormalizeData function within Seurat. Integration of the data was carried out using the FindIntegrationAnchors (dims = 1:25) and IntegrateData (dims = 1:25) functions of Seurat.

The ScaleData and RunPCA functions were executed for Uniform Manifold Approximation and Projection dimensional reduction (dims = 1:25), and the FindNeighbors (dims = 1:25) and

FindClusters (resolution = 1.0) functions were utilized to define clusters. Cell clusters were annotated based on differentially expressed genes (DEGs) identified by the FindAllMarkers function in Seurat. Visualization of DEGs between samples was achieved using the FindMarkers, AverageExpression, and FeaturePlot functions of Seurat, as well as the R packages EnhancedVolcano (ver. 1.16.0) and Nebulosa (ver. 1.8.0). Monocle3 (ver. 1.3.1) and the Slingshot package (ver. 2.2.1) were employed for trajectory analysis. UCell (ver. 1.3.1) was used to compute module enrichment scores. The list of DEGs was ranked by p-value, and GSEA (a collaboration between UC San Diego and the Broad Institute) was conducted using GSEA software version 4.2.2.

In vitro cytotoxic T lymphocyte assay

For the *in vitro* cytotoxic T lymphocyte (CTL) assay, wild-type (WT) and *Fcgr2b*$^{-/-}$ mice were injected with GL261-SIINFEKL. Following the injection of tumor cells into the brain, anti-PD-1 antibody treatment was administered on days 10 and 13 post-injection. On day 15, tumor-infiltrating CD8 T cells were harvested using a MagniSort Mouse CD8 Positive Selection Kit (Invitrogen). The sorted CD8 T cells were then co-cultured with 1×10^4 GL261-OVA-mCherry target cells that had been seeded the previous day at 1:1 and 1:2 target-to-effector cell ratios for 56 hours. Red fluorescent protein levels were measured every 2 hours using the IncuCyte live-cell analysis system (Essen BioScience, Inc., Ann Arbor, MI, USA), and object integrated intensity (OCI) values were calculated.

In vitro stimulation of human PBMCs

The study was conducted according to the guidelines of the Declaration of Helsinki, and approved by the Institutional Review Board of Konyang University Hospital (approval number: KYUH 2020-06-009-008) for the collection of peripheral blood samples from healthy volunteers and the Institutional Review Board of Seoul St. Mary's Hospital (approval number:

KC20TISI0251) for peripheral blood samples from patients. Informed consent from all participants was obtained. Peripheral blood mononuclear cells (PBMCs) were isolated from blood using Lymphocyte Separation Medium (MP Biomedicals, Santa Ana, CA, USA) or Ficoll-Paque PLUS density gradient media (Cytiva, Uppsala, Sweden). 1×10^6 PBMCs per well were cultured in T-cell medium, which consisted of RPMI-1640 supplemented with 10% FBS, 1% penicillin-streptomycin (GenDEPOT), 1% non-essential amino acids (Sigma), 1% sodium pyruvate (WELGENE, Gyeongsan, Korea), 1% HEPES (WELGENE), and 55 μM 2-mercaptoethanol (Gibco, Grand Island, NY, USA). The culture was further supplemented with 300 U/mL of human interleukin-2 (IL-2) (Peprotech, Cranbury, NJ, USA), 1 μg/mL of human anti-CD3 (BD Biosciences, UCHT1), and 1 μg/mL of anti-CD28 (BD Biosciences, CD28.2) antibodies. Cells were incubated at 37°C for 5 days. Following stimulation, transcription factor and cytokine staining procedures were performed as previously described.

Online database analysis

To evaluate the clinical relevance and expression levels of inhibitory receptors, TIMER 2.0 (Tumor Immune Estimation Resource) was employed. The analysis utilized the Gene_Outcome module to evaluate the association between the expression of a particular gene and the hazard ratio through the Cox proportional hazard model. In this study, a panel of inhibitory receptors that can be targeted (PD-1, CTLA4, TIM4, LAG3, and TIGIT), along with FcγRIIB, were examined in 41 diverse cancer types. The top 20 cancer types were ranked according to the adjusted p-values and then represented graphically as volcano plots.

Data availability statement

scRNA-seq data from immune cells in WT and *Fcgr2b*$^{-/-}$ mice treated with anti-PD-1 have been deposited in NCBI's Gene Expression Omnibus under accession code GSE262592.

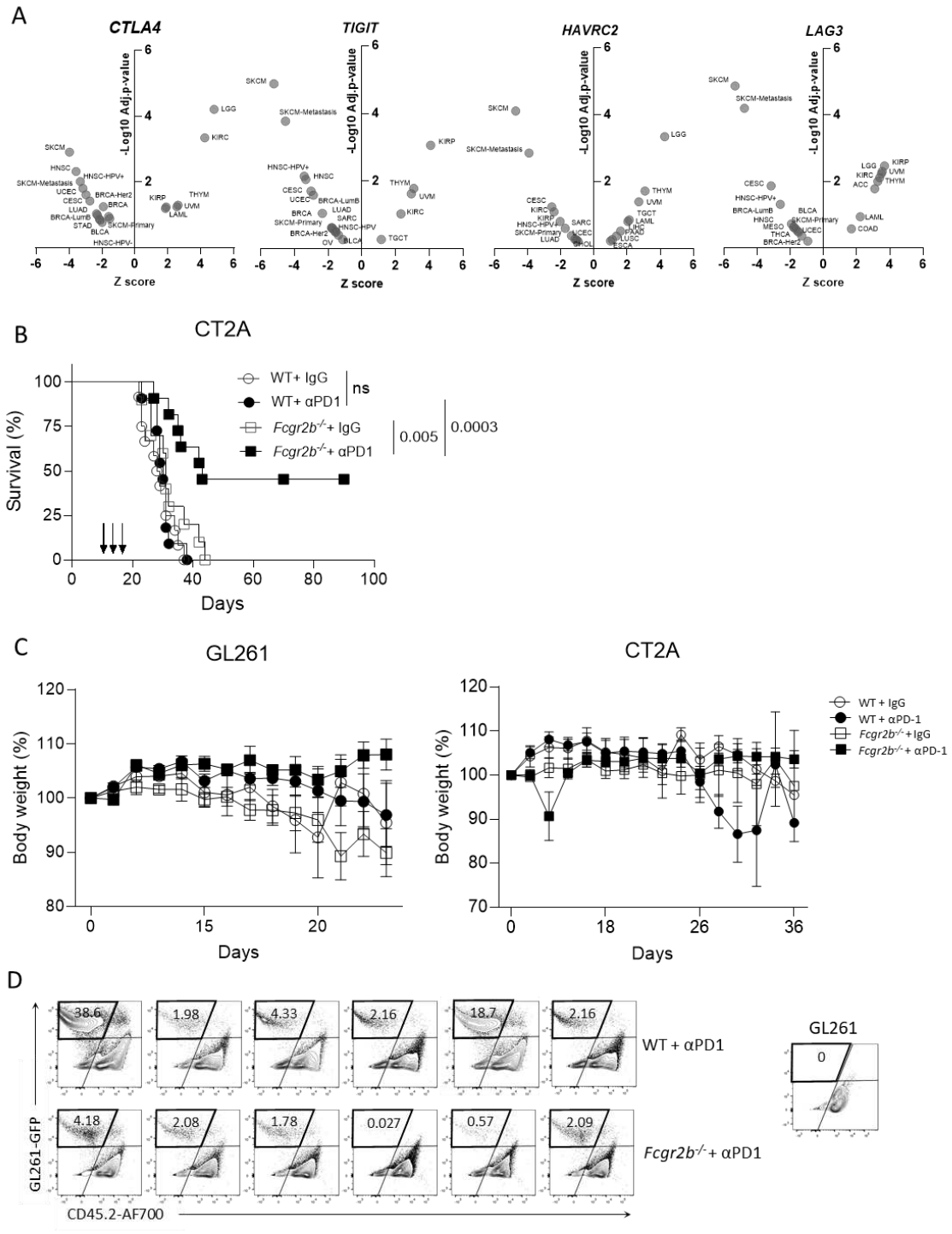

Supplemental figure 1: The synergistic effect of anti-PD-1 treatment in FcγRIIB-deleted mice (related to figure 1).

(A) The hazard ratios were analyzed for *CTLA4, TIGIT, HAVRC2,* and *LAG3* across 35 different

types of cancer. Volcano plots were generated to display the top 20 results based on z-scores and −log10 (p-values).

(B) A CT2A GBM model was assessed in four groups: wild-type (WT) + IgG (n = 12, median survival (MS) = 28.5 days), WT + αPD-1 (n = 11, MS = 30 days), *Fcgr2b*$^{-/-}$ + IgG (n = 10, MS = 31 days), and *Fcgr2b*$^{-/-}$ + αPD-1 (n = 11, MS = 43 days, LTS = 45%).

(C) Body weight variations were observed in GL261- (n = 10) or CT2A- (n = 10) injected WT and *Fcgr2b*$^{-/-}$ mice following treatment with either isotype or anti-PD-1 antibodies.

(D) Flow cytometry plots illustrating GL261-GFP cells at 20 days post-injection. WT (n = 6) and *Fcgr2b*$^{-/-}$ (n = 6) mice were administered anti-PD-1 treatment. LTS, Long-term survival

Mouse experimental results were pooled from or representative of two independent experiments with n = 4–6 mice/group (B–D).

Error bars represent the SEM and the difference in survival was analyzed by the Log-rank (Mantel–Cox) test.

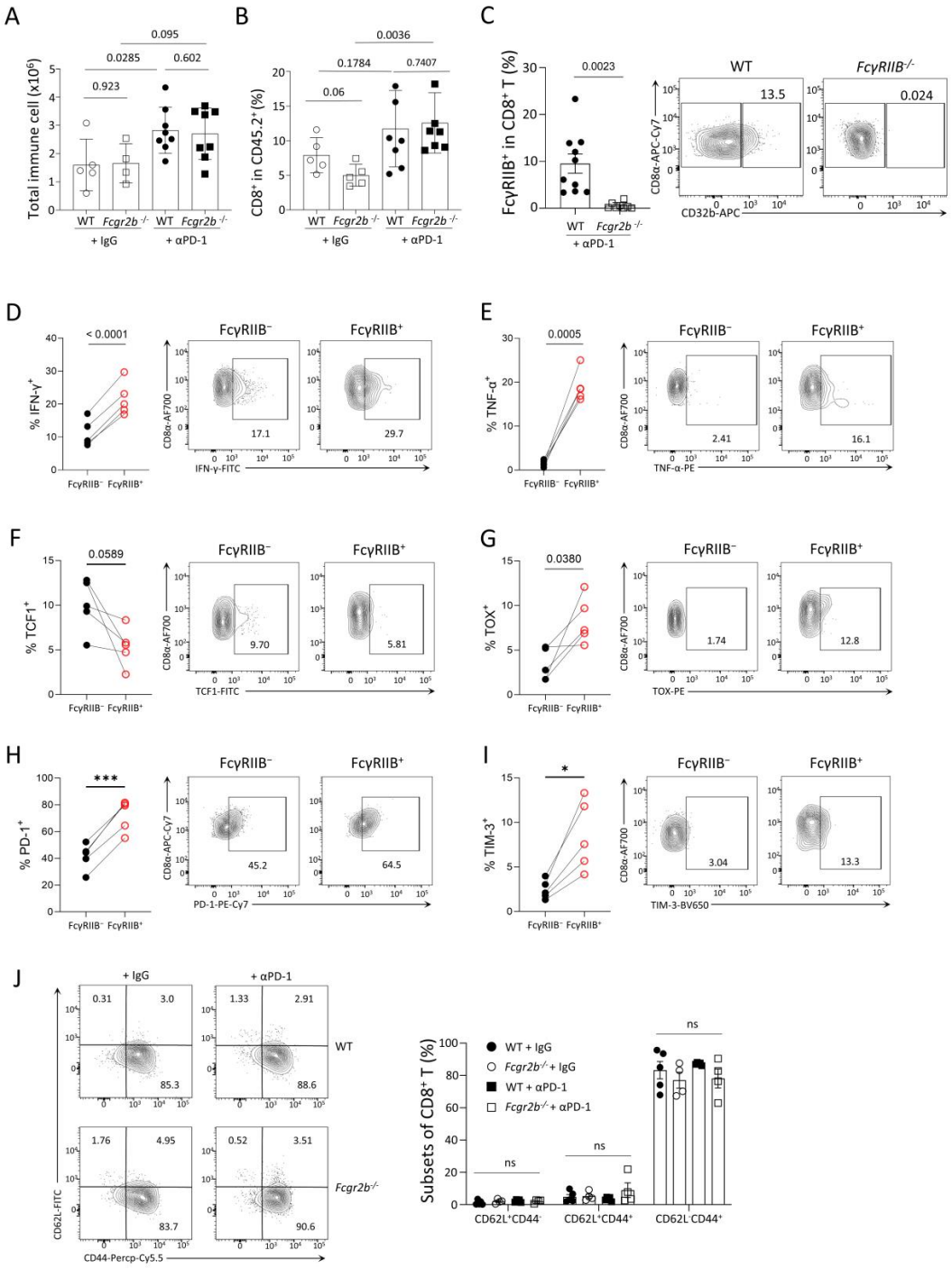

Supplemental figure 2: Expression of FcγRIIB in tumor-infiltrating CD8 T cells and their subset characteristics (related to figure 2).

(A) Total counts of immune cells infiltrating the tumor.

(B) Frequency of CD8 T cells among immune cells.

(C) CD8 T cells expressing FcγRIIB from the brains of GL261-bearing mice were analyzed in wild-type (WT) and *Fcgr2b*$^{-/-}$ mice.

(D–I) Comparisons of FcγRIIB^{-} and FcγRIIB^{+} CD8 T-cell populations from WT mice regarding the expression levels of (D) IFN-γ, (E) TNF-α, (F) TCF1, (G) TOX, (H) PD-1, and (I) TIM-3.

(J) Representative flow cytometry plots and frequency of naïve (CD44^{-}CD62L^{+}), effector (CD44^{+}CD62L^{-}), and central (CD44^{+}CD62L^{+}) memory subsets among tumor-infiltrating CD8 T cells.

All results are representative of two independent experiments, with n = 4–7 mice per group (A–J). Error bars indicate the SEM, and p-values were calculated using two-tailed, paired Student's t-tests (D–I) or unpaired Student's t-tests (A–B, J).

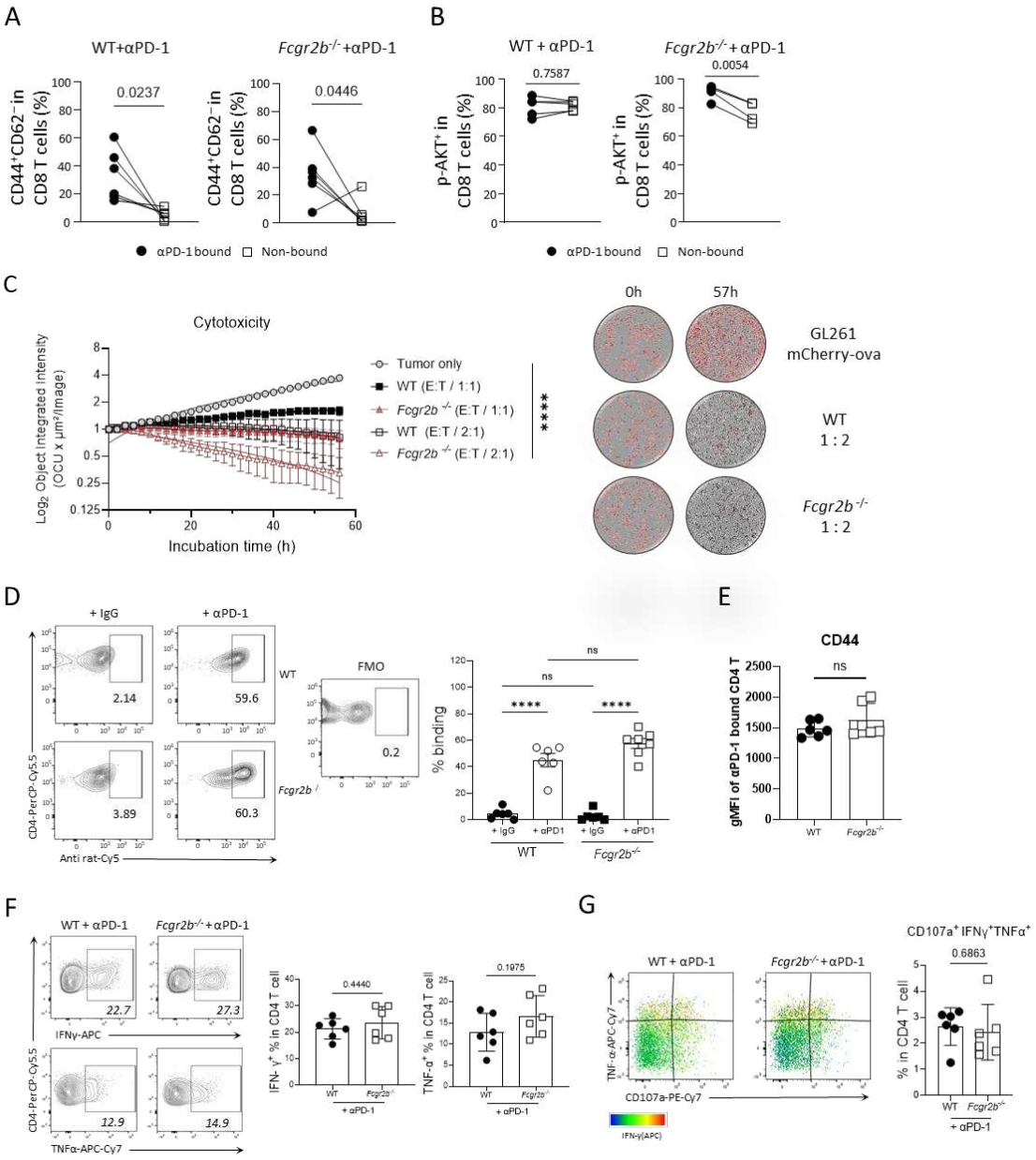

Supplemental figure 3: The augmented anti-GBM response in *Fcgr2b*$^{-/-}$ mice following treatment with anti-PD-1 is mediated by CD8 T cells (related to figure 2).

(A-B) Frequencies of (A) CD44^{+}CD62L^{-} cells and (B) pAKT^{+} cells among tumor-infiltrating CD8 T cells, either bound or unbound to anti-PD-1, were examined.

(C) Real-time cytotoxicity mediated by *ex vivo* purified CD8 T cells from wild-type (WT) and *Fcgr2b*$^{-/-}$ mice was analyzed using GL261-OVA-mCherry target cells in co-culture. Effector-to-target (E:T) ratios of 1:1 and 2:1 were employed, and images were captured every 2 hours over a 57-hour period. Red fluorescence was quantified as object integrated intensity (OCI)

values, and representative images at 0 and 57 hours of incubation time with a 2:1 ratio are presented. The assay was conducted in triplicate wells.

(D) Representative flow cytometry plots and a bar graph are presented to demonstrate the quantification of anti-PD-1 antibody binding on CD4 T cells within tumor tissues. Fluorescence minus one (FMO) was used as a control.

(E) Expression of CD44 in tumor-infiltrating CD4 T cells that bind to anti-PD-1 antibodies.

(F–G) The representative flow cytometry plots and bar graphs illustrate the proportions of (I) IFN-γ^+ or TNF-α^+ CD4 T cells and (J) IFN-γ^+ TNF-α^+ CD107a$^+$ CD4 T cells.

All results were representative of two independent experiments with n = 4–7 mice/group (A–J). Error bars represent the SEM, and p-values were calculated using two-tailed, paired (A, B) or unpaired Student's t-tests (D–G), and simple linear regression analysis (C).

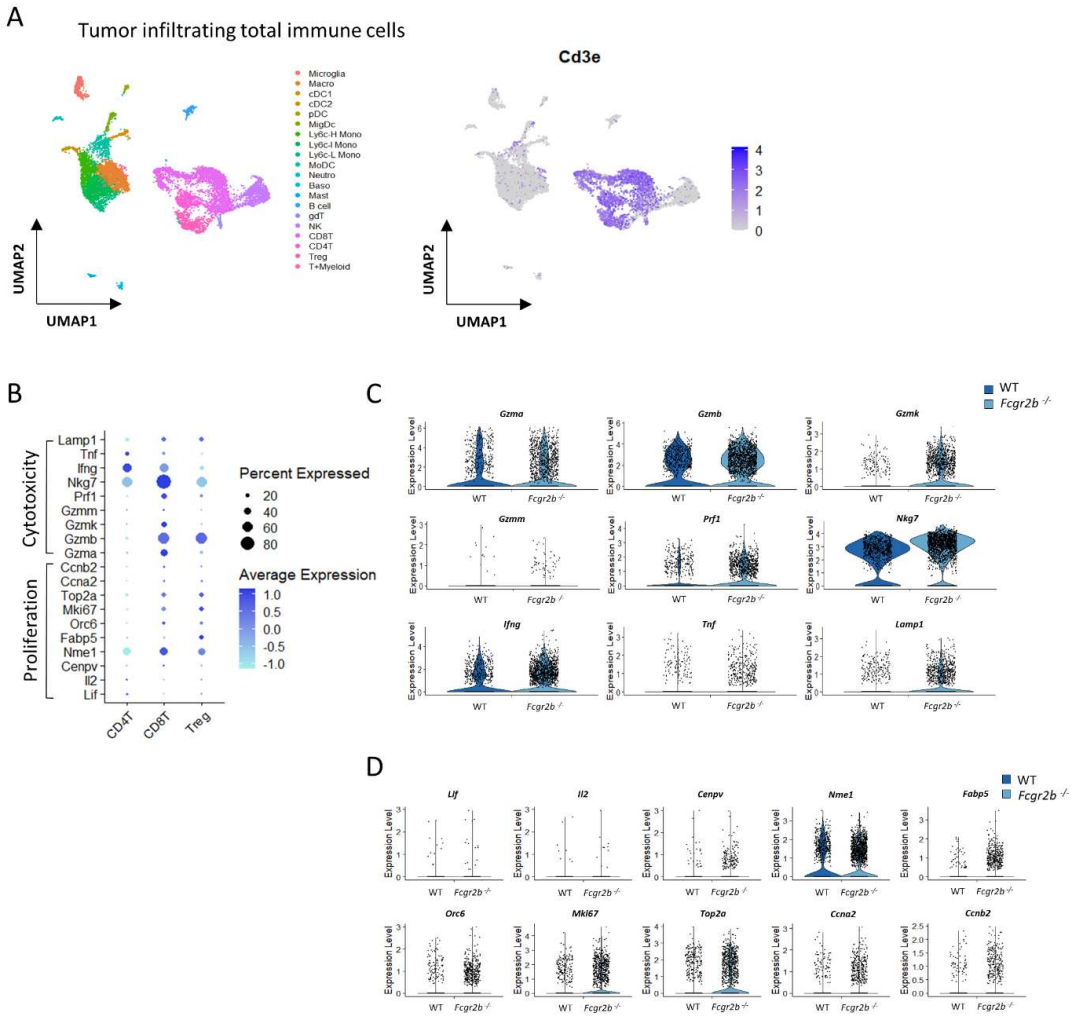

Supplemental figure 4: Transcriptome analysis of tumor-infiltrating immune cells (related to figure 2).

(A) Uniform manifold approximation and projection (UMAP) of annotated immune cell clusters and feature plot of *Cd3e.*

(B) Dotplot for gene sets related to cytotoxicity (*Gzma, Gzmb, Gzmk, Gzmm, Prf1, Nkg7, Ifng, Tnf, Lamp1*) and proliferation (*Lif, Il2, Cenpv, Nme1, Fabp5, Orc6, Mki67, Top2a, Ccna2, Ccnb2*) in CD4, CD8, and regulatory T cells.

(C) Violin plots for individual genes utilized in the cytotoxic scores, as depicted in figure. 2.

(D) Violin plots for individual genes utilized in the proliferation scores, as depicted in figure. 2.

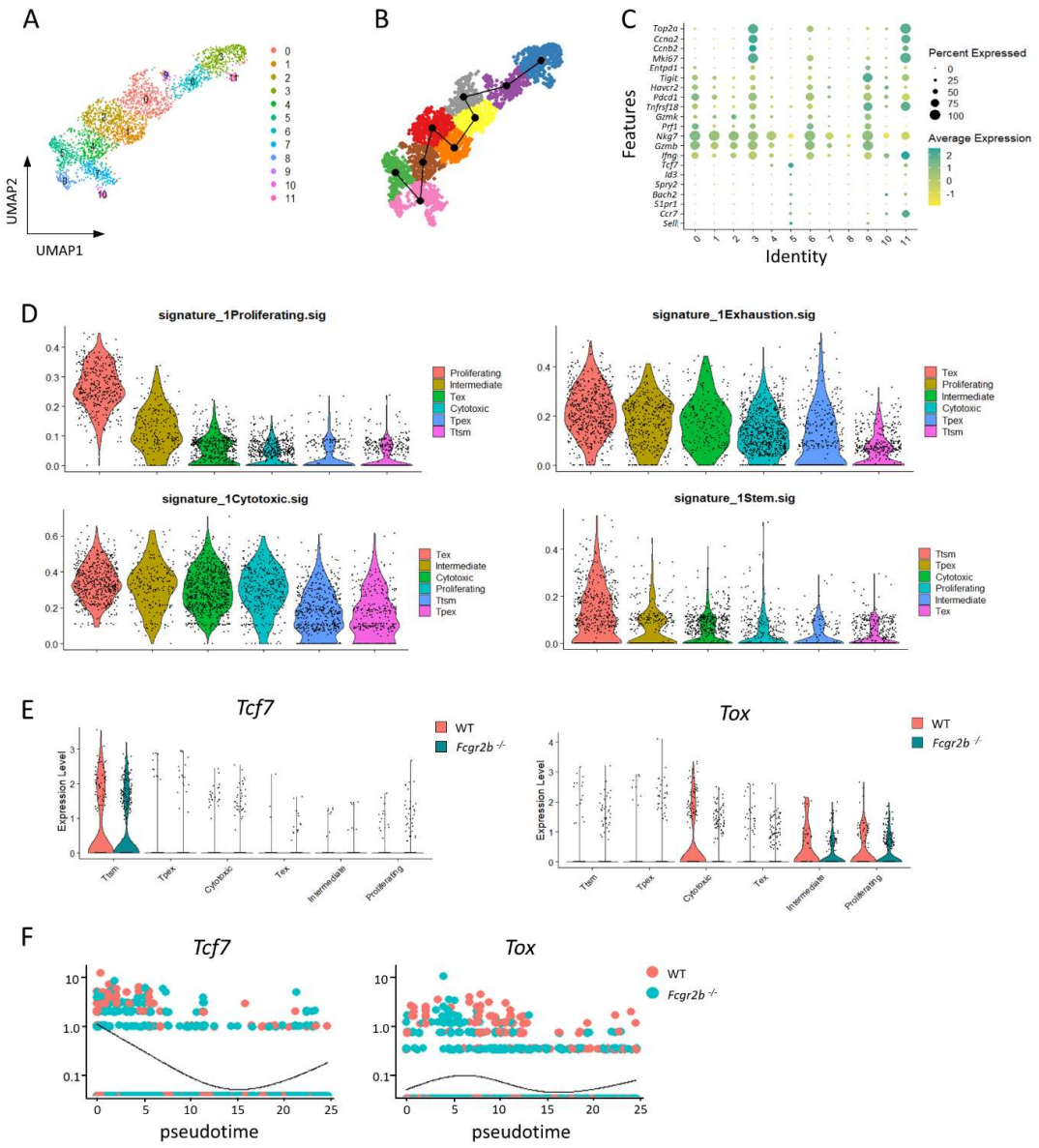

Supplemental figure 5: Transcriptome analysis of tumor-infiltrating CD8 T cells (related to figure 3).

(A) UMAP of 12 clusters of tumor-infiltrating CD8 T cells.

(B) UMAP of CD8 T cells with Slingshot trajectories overlaid.

(C) DotPlot presenting transcript expression of major cell type markers in the specified CD8 T-cell subsets.

(D) Violin plots illustrate the distribution of signature scores as indicated by the cluster. The

proliferation signature comprises *Lif, Il2, Cenpv, Fabp5, Orc6, Mki67, Top2a,* and *Nme1*. The exhaustion signature comprises *Pdcd1, Havcr2, Lag3, Ctla4, Tigit, Cd101, Cx3cr1,* and *Tox*. The cytotoxic signature comprises *Gzma, Gzmb, Gzmk, Prf1, Nkg7, Eomes, Klrg1, Zeb2, Tnf,* and *Ifng*. The stemness signature comprises *Tcf7, Sell, Ccr7, Il7r, S1pr1, Slamf6, Cxcr5,* and *Myb.*

(E) Expression level of *Tcf7* and *Tox* in the CD8 T-cell subcluster.

(F) Pseudotime analysis of the correlation between the expression levels of *Tcf7* and *Tox* and cell progression.

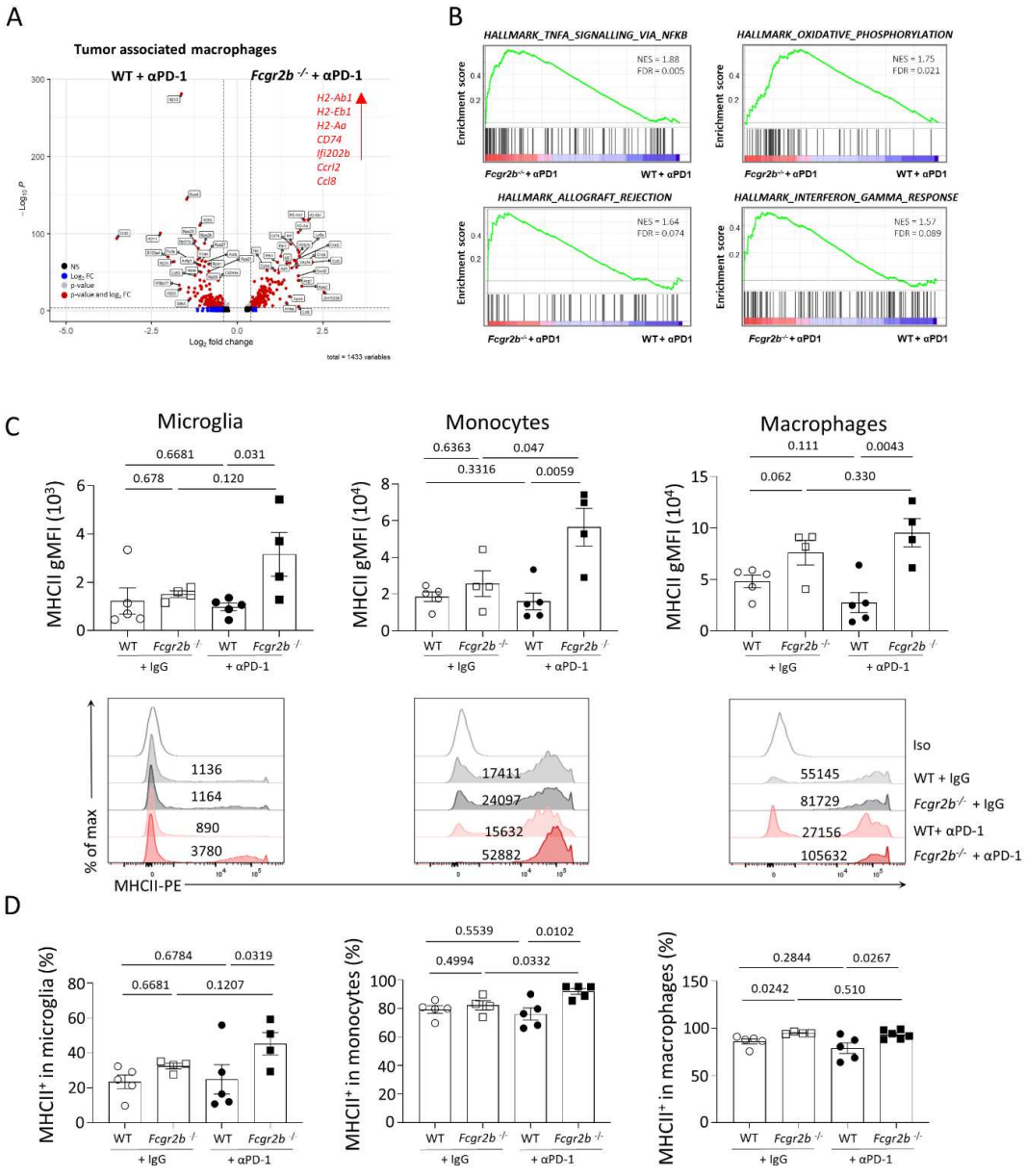

Supplemental figure 6: Transcriptome and protein level analysis of tumor-associated macrophages (TAM) (related to figure 3).

(A–B) Transcriptome analysis was conducted on tumor-associated macrophages (TAMs), which include microglia, monocytes, and macrophages, derived from anti-PD-1-treated wild-type (WT) and *Fcgr2b*$^{-/-}$ mice. (A) The results of the differentially expressed gene (DEG) analysis are displayed in a volcano plot, with significance thresholds established at a p-value

of less than 0.00001 and a Log_2 fold-change greater than 0.5. (B) Based on the DEG results, Gene Set Enrichment Analysis (GSEA) was performed on TAMs, revealing enrichment in the TNF-α/NF-κB pathway, the oxidative phosphorylation pathway, the hallmark allograft rejection pathway, and the hallmark interferon-gamma response pathway within the hallmark gene sets.

(C-D) The FACS analysis of major histocompatibility complex (MHC) class II expression in microglia, monocytes, and macrophages was conducted. The (C) gMFI of MHCII and the (D) frequency of MHCII-positive TAMs were analyzed.

All results were representative of two independent experiments with n = 4–6 mice/group. Error bars represent the SEM, and p-values were calculated using two-tailed unpaired Student's t-tests (C–D).

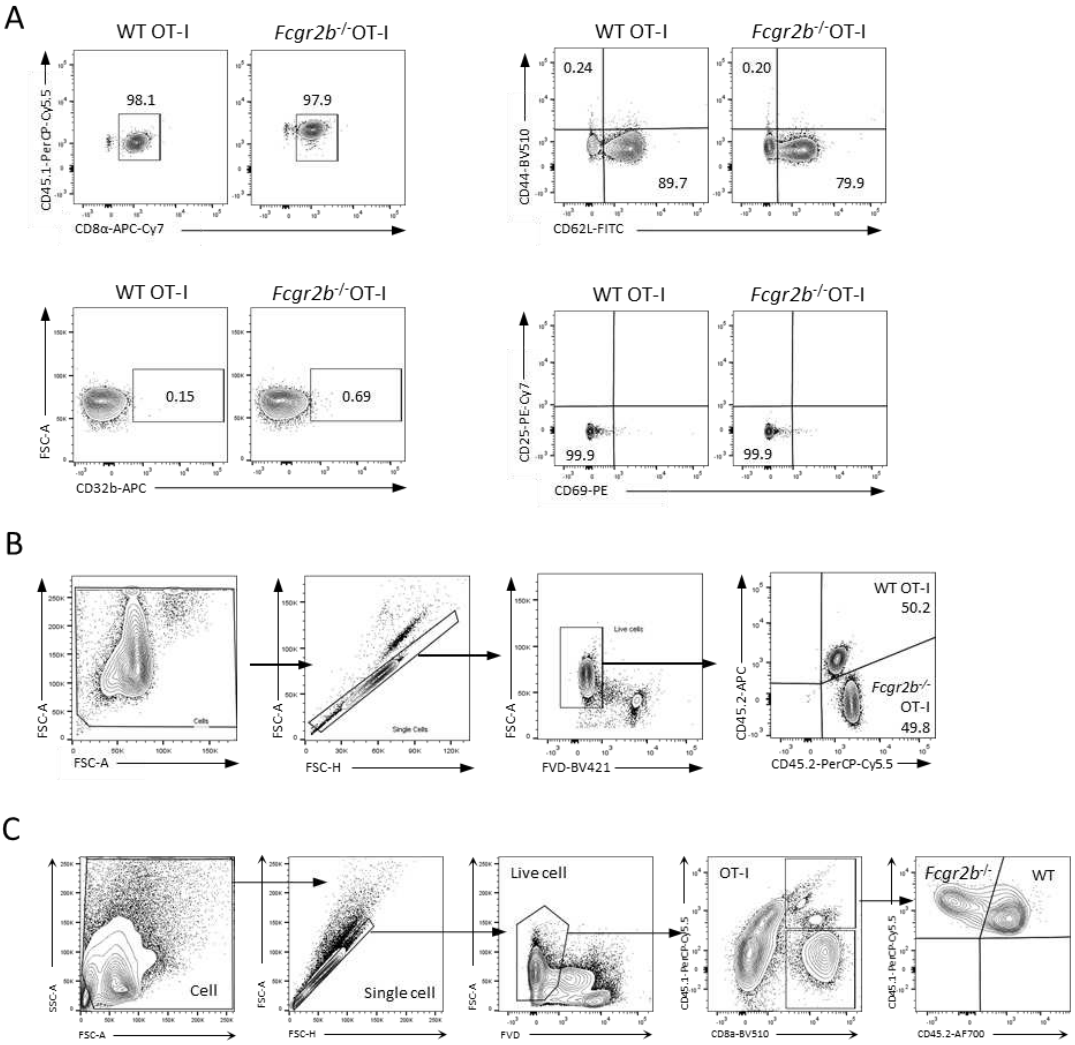

Supplemental figure 7: Adoptive cell transfer of wild-type (WT) and *Fcgr2b*$^{-/-}$ OT-I cells (related to figure 4).

(A) Analysis of purity (CD45.1^{+} CD8α^{+}), activation markers (CD44, CD25, CD69), and FcγRIIB expression on sorted WT and knockout OT-I cells.

(B) Flow plots of WT and *Fcgr2b*$^{-/-}$ OT-I cells prepped for adoptive cell co-transfer.

(C) Gating strategy for tumor-infiltrating WT and *Fcgr2b*$^{-/-}$ OT-I cells.

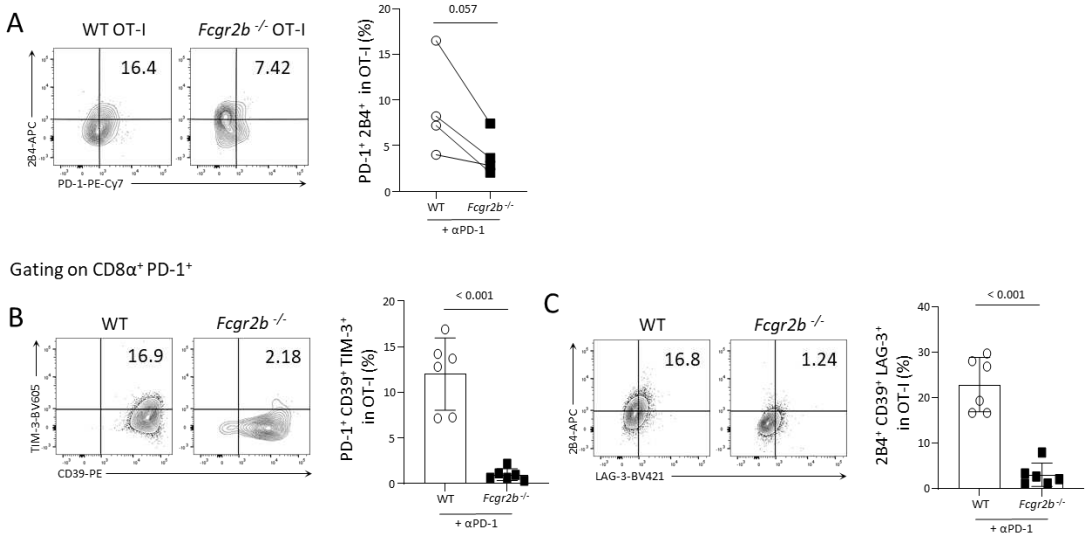

Supplemental figure 8: Expression of inhibitory receptors on tumor-infiltrating wild-type (WT) and *Fcgr2b*$^{-/-}$ OT-I cells and polyclonal CD8 T cells (related to figure 4).

(A) Representative flow plots and a bar graph illustrating the quantification of PD-1^{+} 2B4^{+} WT and *Fcgr2b*$^{-/-}$ OT-I cells from mice injected with GL261-OVA cells (n = 4 per group).

(B–C) Representative flow plots and a bar graph depict the quantification of PD-1^{+} CD39^{+} TIM-3^{+} (B) and 2B4^{+} CD39^{+} LAG-3^{+} (C) WT or *Fcgr2b*$^{-/-}$ CD8 T cells that infiltrated GL261 cell-injected brains (n = 6 per group).

Error bars represent the SEM, and p-values were calculated using paired (A) or unpaired Student's t-tests (B-C).

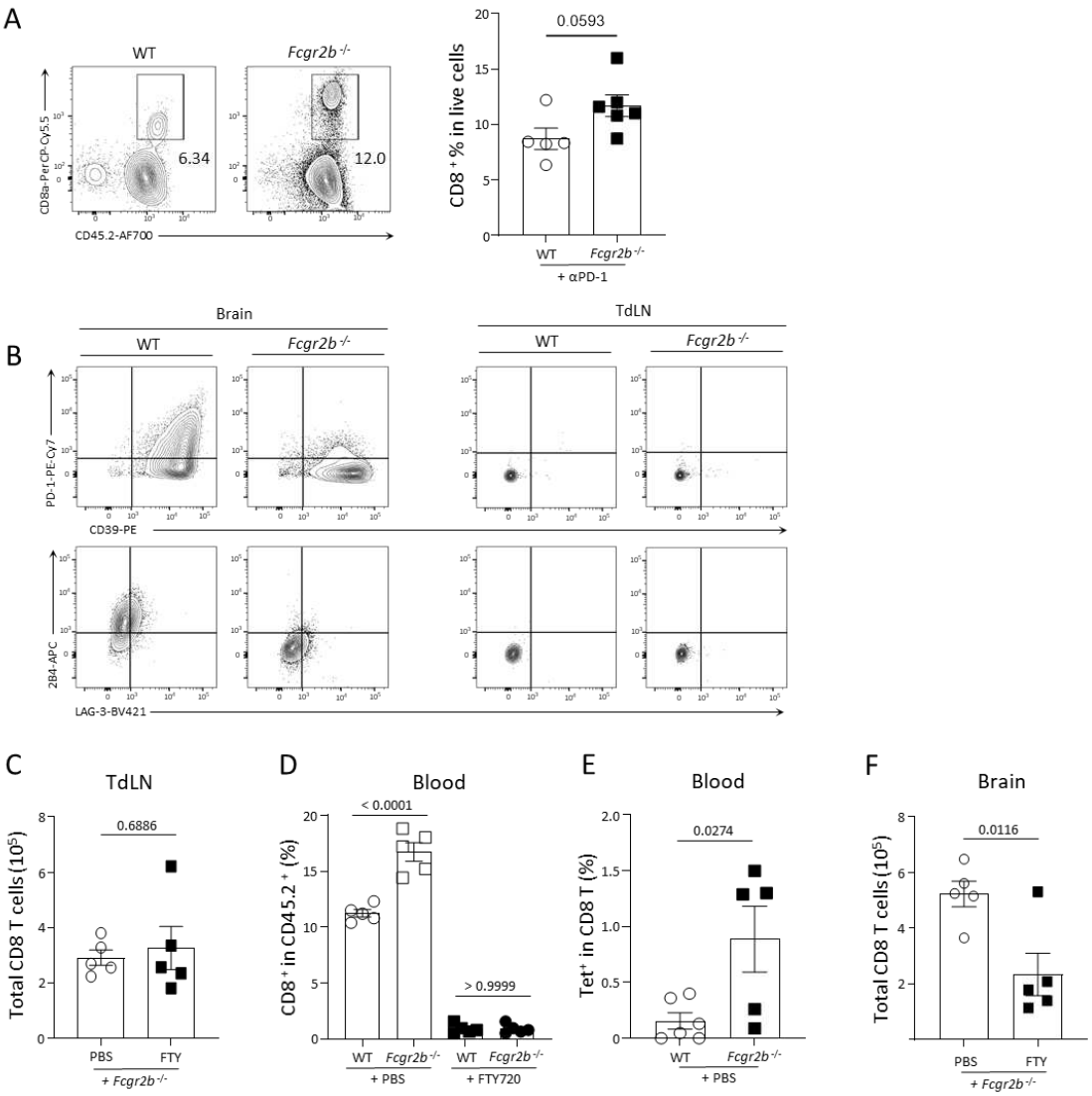

Supplemental figure 9: Analysis of brain tumor-draining deep cervical lymph nodes (related to figure 5).

(A) Representative flow plots and a bar graph illustrating the quantification of CD8 T cells in deep cervical tumor-draining lymph nodes (TdLNs) associated with brain tumors.

(B) Representative flow plots of PD-1$^+$ CD39$^+$ and 2B4$^+$ LAG-3$^+$ CD8 T cells that infiltrated brains injected with GL261 cells and resided in TdLNs.

(C–F) Analysis of CD8 T cells in the tumor-bearing brain, TdLNs, and peripheral blood from GL261-OVA-injected wild-type (WT) and *Fcgr2b*$^{-/-}$ mice treated with anti-PD-1 antibodies and FTY720 (FTY). (C) Quantification of the total number of CD8 T cells from the TdLNs of *Fcgr2b*$^{-/-}$ mice treated with phosphate-buffered saline (PBS) or fingolimod (FTY720). (D) Frequency of CD8 T cells in blood from WT and *Fcgr2b*$^{-/-}$ mice treated with either PBS or

FTY and (E) quantification of Tet^+ CD8 T cells in WT and *Fcgr2b*$^{-/-}$ mice treated with PBS. (F) Total CD8 T cells in tumor-bearing brains treated with FTY720.

Error bars represent the SEM, and p-values were calculated using unpaired Student's t-tests (A, C-F).

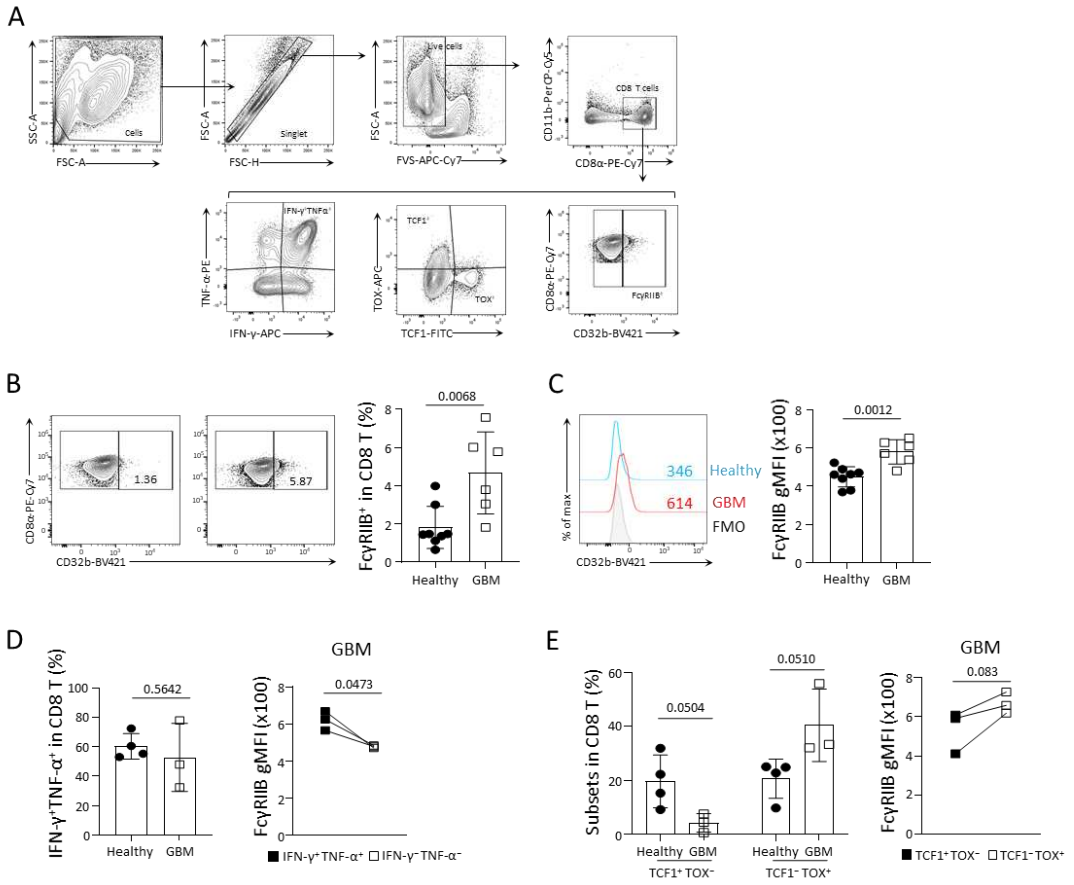

Supplemental figure 10: Expression of FcγRIIB on CD8 T cells and functional characteristics of FcγRIIB$^+$ CD8 T cells in human patients with GBM.

(A–E) PBMCs collected from healthy donors (n = 4) and patients with GBM (n = 3) were stimulated with anti-CD3/CD28 antibodies and human recombinant IL-2 for 5 days. After activation with PMA/ionomycin, CD8 T cells were analyzed for cytokine (IFN-γ and TNF-α) production and TCF-1 and TOX expression levels.

(A) Flow cytometry plots illustrating the gating strategy for the FcγRIIB$^+$ population in human CD8 T cells within PBMCs.

(B–C) Quantification of FcγRIIB$^+$ CD8 T cells in PBMCs from healthy donors and patients with GBM, presented as (B) frequency and (C) gMFI values. All samples were analyzed in duplicate.

(D) The expression levels of IFN-γ and TNF-α were analyzed in healthy donors and patients with GBM. FcγRIIB was examined across IFN-γ$^+$TNF-α$^+$ and IFN-γ$^-$TNF-α$^-$ subsets.

(E) Subsets of CD8 T cells, classified by TCF1 and TOX expression levels (TCF1$^+$TOX$^-$ and TCF1$^-$TOX$^+$), were analyzed in both healthy donors and patients with GBM. The expression of FcγRIIB was evaluated across these subsets.

Error bars represent the SEM, and p-values were calculated using unpaired Student's t-tests. Cell groups originating from the same donor were calculated using the matched-pairs rank test (B–E).

Table S1. Selected gene list for signature scoring analysis (related to figure 3D)

Tumor-specific memory	**Stem-like**	**Exhausted progenitor 1**
Qizhao Huang et al, *Cell 2022*	**Kelli A. Connolly et al, *Science Immunology* 2021**	**Jean-Christophe Beltra, *Immunity* 2020**
Ltb	*Slamf6*	*Tcf7*
Stat1	*Xcl1*	*Slamf6*
Cd69	*Cd200*	*Ptpn6*
Slamf6	*Pdcd4*	*Tuba1b*
Cd27	*Ltb*	*Ighm*
Banf1	*Irf3*	*Ly9*
Tcf7	*Cxcr5*	*Sidt1*
Ccr7		*Emb*
Clec2d		*Ms4a4c*
Stat4		*Sell*
Ikzf1		*Tpm4*
Il7r		*Mndal*
S1pr1		*Cxcr5*
Ddx21		*Dpp4*
Lef1		
Bach2		
C1qbp		
Foxp1		
Sell		

Table S2. List of antibodies for FACS analysis (related to Methods)

Antibodies	Source	Identifier
anti-mouse CD45.2-AF700 (Clone: 104)	BioLegend	Cat# 109822
anti-mouse CD45.2-PE (Clone: 104)	eBioscience	Cat# 12-0454-82
anti-mouse CD45.2-BV421 (Clone: 104)	BD Biosciences	Cat# 562895
anti-mouse CD45.1-Percp-Cy5.5 (Clone: A20)	BD Biosciences	Cat# 560580
anti-mouse CD8α-AF700 (Clone: 53-6.7)	BD Biosciences	Cat# 557959
anti-mouse CD8α-APC-Cy7 (Clone: 53-6.7)	BioLegend	Cat# 100714
anti-mouse CD4-Percp-Cy5.5 (Clone: RM4.5)	BD Biosciences	Cat# 550954
anti-mouse CD11b-BV510 (Clone: M1/70)	BioLegend	Cat# 101263
anti-mouse PD-1-PECy7 (Clone: RMPI1-30)	BioLegend	Cat# 109109
anti-mouse TIM-3-BV650 (Clone: 25F.1D6)	BD Biosciences	Cat# 755162
anti-mouse CD39-PE (Clone: Duha59)	BioLegend	Cat# 143803
anti-mouse CD244-APC (Clone: m2B4 (B6)458.1)	BioLegend	Cat# 133517
anti-mouse LAG-3-BV421 (Clone: C9B7W)	BioLegend	Cat# 125221
anti-mouse CD44-Percp-Cy5.5 (Clone: IM7)	BioLegend	Cat# 103032
anti-mouse CD44-BV510 (Clone: IM7)	BD Biosciences	Cat# 563114
anti-mouse CD62L-FITC (Clone: MEL-14)	BioLegend	Cat# 104406
anti-mouse OVA-Kb tetramer-APC	MBL	Cat# TS-5001-2C
anti-mouse & human TCF-1-AF488 (Clone: C63D9)	Cell signaling Technology	Cat# 6444S
anti-mouse TOX-PE (Clone: TXRX10)	Thermo Fisher Scientific	Cat# 12-6502-82
anti-mouse & human TOX-APC (Clone: REA473)	Miltenyi Biotech	Cat# 130-118-335
anti-mouse Ki67-FITC (Clone: 16A8)	BioLegend	Cat# 652410
anti-mouse Ki67-PE (Clone: SolA15)	Thermo Fisher Scientific	Cat# 12-5698-82
anti-mouse IFN-γ-APC (Clone: XMG1.2)	BioLegend	Cat# 505810
anti-mouse TNF-α-APC-Cy7 (Clone: MP6-XT22)	BioLegend	Cat# 506343
anti-mouse CD107a-PE-Cy7 (Clone: ID4B)	BD Biosciences	Cat# 560647
anti-mouse Tmem119-FITC (Clone: V3RT1GOsz)	Thermo Fisher Scientific	Cat# 53-6119-82
anti-mouse Ly-6C-APC (Clone: HK1.4)	BioLegend	Cat# 128016
anti-mouse F4/80-PE-Cy7 (Clone: BM8)	BioLegend	Cat# 123114
anti-mouse MHC Class II-PE (Clone: M5/114.15.2)	Thermo Fisher Scientific	Cat# 12-5321-82
anti-mouse pAKT-APC (Clone: SDRNR)	Thermo Fisher Scientific	Cat# 17-9715-42
anti-human CD32b-BV421 (Clone: FLI8.26)	BD Biosciences	Cat# 564838
anti-human CD8- PE-Cy7 (Clone: RPA-T8)	BD Biosciences	Cat# 557746
anti-human IFN-γ-APC (Clone: B27)	BD Biosciences	Cat# 562017
anti-human TNF-α-APC (Clone: Mab11)	BD Biosciences	Cat# 554513